IJCFD, 1999, Vol. 11, pp. 261–273
Reprints available directly from the publisher
Photocopying permitted by license only

Non-Symmetric Convective Flows in Laterally Heated Rectangular Cavities

A. YU. GELFGAT*, P. Z. BAR-YOSEPH and A. L. YARIN

Computational Mechanics Laboratory, Department of Mechanical Engineering, Technion - Israel Institute of Technology, Haifa 32000, Israel

(Received in final form 30 August 1998)

Bifurcations of central symmetry breaking and stability of nonsymmetric states of buoyancy-driven convection in laterally heated cavities are studied numerically. The calculations are carried out using two independent numerical approaches. Stability and weakly nonlinear analysis of the calculated bifurcations are studied by the spectral Galerkin method. Time-marching calculations are carried out using the finite volume method. By applying two independent numerical approaches the subcritical steady flows, their stability, the transitions between different states and flows at small and large supercriticalities are comprehensively investigated. It is shown how these numerical techniques can be applied for interpreting a particular experimental result.

Keywords: Convective flows, stability, bifurcation, spectral Galerkin method, buoyancy-driven convection

1. INTRODUCTION

Oscillatory instability of steady convection in laterally heated rectangular cavities is a well-known problem which has significant practical importance [1, 2]. At the same time it is used as a convenient benchmark problem in computational fluid mechanics and heat transfer [1]. Special interest in the convection of low Prandtl number fluids is connected with the stability of melt flow in crystal growth processes. It was shown recently [3–6] that stability properties of such flows strongly depend on the Prandtl number, aspect ratio of the cavity and boundary conditions. In particular, it was shown that at certain values of the aspect ratio and the Prandtl number, the first instability of the flow is a central-symmetry-breaking steady bifurcation which results in a steady nonsymmetric flow [4, 6]. The latter becomes oscillatory unstable at larger values of the Grashof number. Such central-symmetry breaking bifurcations are the main objective of the present numerical study.

Two independent numerical approaches are applied for numerical solution of the system of the Boussinesq equations of buoyancy driven convection. The stability analysis is carried out

* Corresponding author.

by the spectral Galerkin method with globally defined basis functions. This permits a significant reduction of a number of degrees of freedom of the corresponding dynamical system and reduces solution to the eigenvalue problem associated with the linear stability of the fluid flow [7, 8]. The straight-forward time-marching calculations are carried out using the finite volume method [9]. These calculations play the role of a numerical experiment and permit to validate results of the stability analysis and to calculate supercritical oscillatory flows at large supercriticalities, as well as the cases of subcritical bifurcations.

Application of this numerical technique is illustrated on the model problem of convection of a fluid with zero Prandtl number. In spite of the fact that this model cannot always be used for the modeling of stability of realistic fluid flows with low but finite Prandtl number [3–6] it remains a convenient benchmark problem and permits to validate the described numerical approach. However, to compare with experiment (where the Prandtl number is always finite) we switch to calculations with the finite Prandtl number corresponding to the experimental liquid. In the present work, for example, the numerical technique developed is used for interpretation of the experimental result of [10] obtained for oscillatory instability of convection of mercury (whose Prandtl number Pr = 0.026 is small but finite) in a cavity with the height:length:width ratio equal to 1:8:8. To the best of our knowledge this result has not yet been explained completely in any other study.

The article is organized as follows. Section 2 contains the formulation of the problem. Some relevant peculiarities of the numerical methods involved are presented in Section 3. Results and discussion are presented in Section 4. The conclusions are drawn in Section 5.

2. FORMULATION OF THE PROBLEM

The convective flow in a rectangular cavity $0 \le x \le A$, $0 \le y \le 1$ is described by the dimensionless momentum, energy and continuity equations for Newtonian Boussinesq fluid

$$\frac{\partial \mathbf{v}}{\partial t} + (\mathbf{v} \cdot \nabla)\mathbf{v} = -\nabla p + \Delta \mathbf{v} + \mathrm{Gr}\,\theta\,\mathbf{e}_y \qquad (1)$$

$$\frac{\partial \theta}{\partial t} + (\mathbf{v} \cdot \nabla)\theta = \frac{1}{\mathrm{Pr}}\Delta\theta, \quad \nabla \cdot \mathbf{v} = 0 \qquad (2,3)$$

Here $\mathbf{v}$ is the fluid velocity, θ is the temperature, p is the pressure, $\mathrm{Gr} = \bar{g}\bar{\beta}(\bar{\theta}_1 - \bar{\theta}_2)\bar{H}^3/\bar{\nu}^2$ is the Grashof number, $\mathrm{Pr} = \bar{\nu}/\bar{\chi}$ is the Prandtl number, $A = \bar{L}/\bar{H}$ is the aspect ratio, $\bar{g}$ is the gravity acceleration, $\bar{\beta}$ is the thermal expansion coefficient, $(\bar{\theta}_1 - \bar{\theta}_2)$ is the temperature difference between the cold and hot vertical walls, $\bar{\nu}$ is the kinematic viscosity, $\bar{\chi}$ is the thermal diffusivity, $\bar{L}$ and $\bar{H}$ are respectively the length and the height of the cavity (the overbar indicates dimensional variables).

The boundary conditions correspond to the Ra–Ra case of the benchmark defined in [1]. No-slip boundary conditions for velocity are imposed on all four boundaries:

$$\begin{aligned}\mathbf{v}(x = 0, 0 \le y \le 1) &= \mathbf{v}(x = A, 0 \le y \le 1)\\ &= \mathbf{v}(y = 0, 0 \le x \le A)\\ &= \mathbf{v}(y = 1, 0 \le x \le A) = \mathbf{0},\end{aligned} \qquad (4)$$

vertical boundaries are isothermal:

$$\begin{aligned}\theta(x = 0, 0 \le y \le 1) &= 1,\\ \theta(x = A, 0 \le y \le 1) &= 0,\end{aligned} \qquad (5,6)$$

and horizontal boundaries are thermally insulated:

$$\begin{aligned}&\frac{\partial \theta}{\partial y}(y = 0, 0 \le x \le A)\\ &= \frac{\partial \theta}{\partial y}(y = 1, 0 \le x \le A) = 0.\end{aligned} \qquad (7)$$

3. NUMERICAL PROCEDURES

3.1. Spectral Galerkin Method

The Problem (1)–(7) was solved using the spectral Galerkin method with the globally defined basis

functions which were proposed in [7]. The velocity and the temperature are approximated by the truncated series

$$\mathbf{v} \approx \sum_{i=0}^{N_x}\sum_{j=0}^{N_y} c_{ij}(t)\mathbf{u}_{ij}(x,y),$$
$$\theta = (1-x) + \sum_{i=0}^{M_x}\sum_{j=0}^{M_y} d_{ij}(t)q_{ij}(x,y). \tag{8}$$

Here $c_{ij}(t)$ and $d_{ij}(t)$ are unknown time-dependent coefficients, N_x, N_y, M_x, M_y are numbers of basis functions used for the approximation in the x- and y- directions. The basis functions $\mathbf{u}_{ij}(x,y)$ and $q_{ij}(x,y)$ are defined as

$$\mathbf{u}_{ij}(x,y) = \left\{ \begin{array}{l} \displaystyle\sum_{m=0}^{4} \frac{a_{im}}{2(i+m)} T_{i+m}\left(\frac{x}{A}\right) \sum_{l=0}^{4} b_{jl} U_{j+l-1}(y) \\ \displaystyle -\sum_{m=0}^{4} a_{im} U_{i+m-1}\left(\frac{x}{A}\right) \sum_{l=0}^{4} \frac{b_{jl}}{2(j+l)} T_{j+l}(y) \end{array} \right\}, \tag{9}$$

$$q_{ij}(x,y) = \sum_{m=0}^{2} p_{im} T_{i+m}\left(\frac{x}{A}\right) \sum_{l=0}^{2} q_{jl} T_{j+l}(y). \tag{10}$$

Here T_n and U_n are the Chebyshev polynomials of the first and the second type respectively

$$T_n(x) = \cos[n \arccos(2x-1)],$$
$$U_n(x) = \frac{\sin[(n+1)\arccos(2x-1)]}{\sin[\arccos(2x-1)]}. \tag{11}$$

The relation between the Chebyshev polynomials $(d/dx)T_{n+1}(x) = 2(n+1)U_n(x)$ yields $\nabla \cdot \mathbf{u}_{ij} = 0$. Therefore the approximation of the velocity (8) is analytically divergence-free for any number of Galerkin modes.

Coefficients a_{im}, b_{jl}, p_{im} and q_{jl} are defined with the help of computer algebra such that all the boundary conditions (4)–(7) are satisfied analytically. The expressions for the coefficients a_{im}, b_{jl}, p_{im} and q_{jl} for different types of boundary conditions are reported in [7].

Application of the Galerkin method excludes the pressure gradient from the Navier–Stokes equation (1) (since $\langle \nabla p, \mathbf{u}_{ij} \rangle = 0$ for divergent-free vectors $\mathbf{u}_{ij}$ satisfying the no-slip boundary conditions) and reduces the Problems (1)–(7) to a system of ordinary differential equations (ODEs) for the time-dependent coefficients $c_{ij}(t)$ and $d_{ij}(t)$ that can be written in the following form (the summation convention on repeated indices is assumed):

$$\tilde{S}_{ij}\dot{X}_i = \tilde{S}_{ij}\frac{dX_i(t)}{dt} = \tilde{F}_i(\mathbf{X}(t), \mathrm{Gr}, \mathrm{Pr}, A)$$
$$= \tilde{L}_{ij}X_j + \tilde{N}_{ijk}X_jX_k + \tilde{Q}_i. \tag{12}$$

Here $i, j, k = 1, 2, \ldots, (N_x+1)(N_y+1) + (M_x+1)(M_y+1)$ and

$$\left.\begin{array}{ll} X_{i(M_y+1)+j+1} = d_{ij}, & 0 \le i \le M_x; 0 \le j \le M_y \\ X_{(M_x+1)(M_y+1)+i(N_y+1)+j+1} = c_{ij}, & 0 \le i \le N_x; 0 \le j \le N_y \end{array}\right\} \tag{13}$$

Matrices $\tilde{L}_{ij}$, $\tilde{N}_{ijk}$, $\tilde{Q}_i$ contain coefficients of all linear, bilinear and free terms of the equations, respectively. The Gram matrix $\tilde{S}_{ij} = \langle \mathbf{u}_i, \mathbf{u}_j \rangle \neq I$ (I is the identity matrix) arises because the basis functions are not orthonormal. Multiplication of the left and the right hand sides of (12) by the inverse matrix $\tilde{S}_{ij}^{-1}$ reduces the dynamical system to the following explicit form:

$$\dot{X}_i = \frac{dX_i(t)}{dt} = F_i(\mathbf{X}(t), \mathrm{Gr}, \mathrm{Pr}, A)$$
$$= L_{ij}X_j + N_{ijk}X_jX_k + Q_i \tag{14}$$

A possible ill-conditioning of the Gram matrix $\tilde{S}_{ij}$ was checked by calculating the inverse matrix $\tilde{S}_{ij}^{-1}$ with single, double and quadruple precisions, and by the orthonormalization of the basis functions (9) with Gram–Schmidt procedure. No significant changes in the results were found. Therefore, it was concluded that the Gram matrix $\tilde{S}_{ij}$ is well defined and all further calculations were carried out using the explicit form (14) of the dynamical system, which was calculated with the double precision arithmetic.

The explicit form of system (14) permits to use standard numerical methods developed for ODEs both for obtaining stationary and non-stationary

solutions and for investigating the stability of solutions. If $\mathbf{X} = \mathbf{X}^0$ is a steady solution of (14) then its linear stability is defined by the eigenvalues of the Jacobian matrix

$$J_{mk} = \frac{\partial \dot{X}_m}{\partial X_k} = L_{mk} + (N_{mkn} + N_{mnk})X_n^0 \qquad (15)$$

The steady solution $\mathbf{X} = \mathbf{X}^0$ is unstable if there exists at least one eigenvalue of J_{mk} with a positive real part. The study of stability requires to determine a value of Gr such that the real part of the dominant eigenvalue (eigenvalue with the maximal real part) $\Lambda = \Lambda^r + i\Lambda^i$ is zero: $\Lambda^r = 0$ and $\partial\Lambda^r/\partial \mathrm{Gr} \neq 0$. If $\Lambda^i = 0$ then a bifurcation from one steady solution to another can be expected. If $\Lambda^i \neq 0$ then a bifurcation to a periodic solution, called Hopf bifurcation [11, 12] takes place. In the latter case $\omega_{cr} = \Lambda^i$ estimates the circular frequency of the oscillatory solution which branches from the steady state after the onset of the oscillatory instability. The most unstable perturbation of the dynamical system (14) is defined by eigenvector $\mathbf{V}$ corresponding to the dominant eigenvalue Λ with $\Lambda^r = 0$ ($J_{mk}V_k = \Lambda V_m = i\Lambda^i V_m$). Components of the eigenvector $\mathbf{V}$ redefined as the coefficients c_{ij} and d_{ij} from (13), define the expansion of the most unstable perturbation of the flow in the Galerkin series (8). Similarly the limit cycle of the dynamical system (14), which develops as a result of Hopf bifurcation, defines as approximation of the periodic solution of Problem (1–7).

If at $\mathrm{Gr} = \mathrm{Gr}_{cr}$ the Hopf bifurcation takes place then the branching oscillatory state may be asymptotically approximated as [8, 12]

$$\mathrm{Gr} = \mathrm{Gr}_{cr} + \mu\varepsilon^2 + O(\varepsilon^4), \qquad (16a)$$

$$T(\mathrm{Gr}) = \frac{2\pi}{\omega_{cr}}[1 + \tau\varepsilon^2 + O(\varepsilon^4)], \qquad (16b)$$

$$\mathbf{X}(t;\mathrm{Gr}) = \mathbf{X}^0(\mathrm{Gr}_{cr}) + \varepsilon \mathrm{Real}\left[\mathbf{V}\exp\left(\frac{2\pi i}{T}t\right)\right] + O(\varepsilon^2). \qquad (16c)$$

Here ε is a formal positive parameter, $(\mathrm{Gr} - \mathrm{Gr}_{cr})$ is the supercriticality, ω_{cr} is the critical circular frequency, T is the period of oscillations, and $\mathbf{X}$ is the asymptotic solution of ODE system (14) for the Grashof number defined in (16a). The asymptotic expansion (16) is defined by two parameters μ and τ, which are calculated using the algorithm of [12]. Details of the applications of this algorithm to a dynamical system written in the form (14) are given in [8]. The Floquet exponent, which defines the stability of the branching limit cycle, can be asymptotically approximated as [12]:

$$\beta = -2\mu\varepsilon^2 \frac{\partial\Lambda^r}{\partial \mathrm{Gr}}\bigg|_{\mathrm{Gr}=\mathrm{Gr}_{cr}} \qquad (17)$$

Growth of Λ^r with the increase of Gr yields $\partial\Lambda^r/\partial\mathrm{Gr} > 0$, which means that the limit cycle (16) is stable if $\mu > 0$ (supercritical bifurcation, $\beta < 0$), and is unstable if $\mu < 0$ (subcritical bifurcation, $\beta > 0$).

The calculations by the Galerkin method are arranged in the following way: first, for an initial value of the Grashof number Gr^0 a stationary solution of ODE system (14) is calculated by the Newton method; then the eigenvalues of the Jacobian matrix (15) are calculated using the QR decomposition algorithm. These two steps are repeated for the next value of the Grashof number $\mathrm{Gr}^1 > \mathrm{Gr}^0$. Then the real part of the dominant eigenvalue Λ^r is considered as a function of Gr, and the critical value of the real Grashof number is calculated as a solution of the equation $\Lambda^r(\mathrm{Gr}_{cr}) = 0$, which is solved with the secant method. The QR decomposition algorithm is chosen due to its independence on the condition number of the matrix. This algorithm requires the calculation of all eigenvalues in order to find the dominant one. To reduce the amount of computations we tried to use the Arnoldi iteration algorithm for calculating the dominant eigenvalue only. However, it was found that correct results can be ensured only when the number of the Krylov basis vectors approaches the dimension of the Jacobian matrix J_{mk}. This makes the Arnoldi iteration less effective

as compared to the standard QR decomposition algorithm. A possible reason for this is the non-sparse structure of J_{mk}.

Various test calculations of steady state flows and the onset of oscillatory instability were reported in [3–7] and are not contained here. The test calculations included study of convergence of the Galerkin series (8), comparison with numerical data available in the literature and with the calculations based on the finite volume method.

3.2. Finite Volume Method

The finite volume method was chosen for time-marching computations since it provides conservative numerical schemes (conservation of mass, momentum and energy). This property is essential for the numerical study in the vicinity of critical stability points.

The finite volume schemes are of second order in space and time. The SIMPLE algorithm [9] is applied together with the second-order three-time-level approximation of the time derivative [13]. The finite volume method is used for two main purposes: to validate the stability results obtained by the Galerkin method and to calculate supercritical unsteady flows for large supercriticalities and in the case of subcritical bifurcations.

The finite volume method is formulated for a general non-uniform staggered grid. However the present calculations are carried out with the use of uniform grid only. The choice of uniform grids is motivated by the initially unknown number of convective rolls and the possibility of multiple steady and oscillatory solutions [4–6]. Since any possible number of convective rolls and any possible breaks of symmetry are allowed, the spatial discretization should be uniform. Thus, uniform grids appear to be the most reasonable choice.

4. RESULTS

The Problem (1–7) is symmetric with respect to simultaneous change of the direction of the gravity force and the replacement of the hot and cold vertical boundaries. It follows from this symmetry that if a solution $\{v_0(x, y, t), \theta_0(x, y, t)\}$ exists then $\{-v_0(A-x, 1-y, t), \ 1-\theta_0(A-x, 1-y, t)\}$ is another solution of the same problem. Both solutions coincide if they are centrally symmetric. Obviously, at low Grashof numbers a single centrally symmetric solution exists. However, at higher Grashof numbers a central symmetry breaking bifurcation can take place, such that a steady central symmetric solution becomes non-symmetric (steady or oscillatory). These bifurcations are characterized by the two-sided pitchfork. Depending on the initial state, the resulting flow approaches a particular branch of the pitchfork. Figure 1 shows the calculated regions where the steady pitchfork bifurcations of central-symmetry-breaking were found. It was shown [4–6] that in cavities with four no-slip boundaries there exist multiple steady state solutions which differ by the number of convective rolls. For the case of $\mathrm{Pr} = 0$ and $1 < A < 10$, considered here, a steady symmetry-breaking bifurcation was found for each of the branches containing one, two, three, and four primary convective rolls. Examples of steady symmetry and non-symmetric flow patterns are shown in Figures 2–5.

The non-symmetric steady state flows are stable inside the shadowed regions shown in Figures 1(a)–(d). Lower boundaries of the shadowed regions in Figures 1(a)–1(d) correspond to the steady pitchfork bifurcation from the centrally symmetric to the non-symmetric steady state flows. Upper boundaries of the shadowed regions correspond to the oscillatory instability of the non-symmetric steady state flows. The neutral curves aside the shadowed regions correspond to the oscillatory instability of the centrally symmetric steady state flows. In the cases of single-, two-, and three-roll steady states (Figs. 1(a)–(c)) the steady pitchfork bifurcation is supercritical, such that the lower boundary of the corresponding shadowed region conforms to the stability of both symmetric and non-symmetric states. In the case of four-roll steady state flows the bifurcation is subcritical,

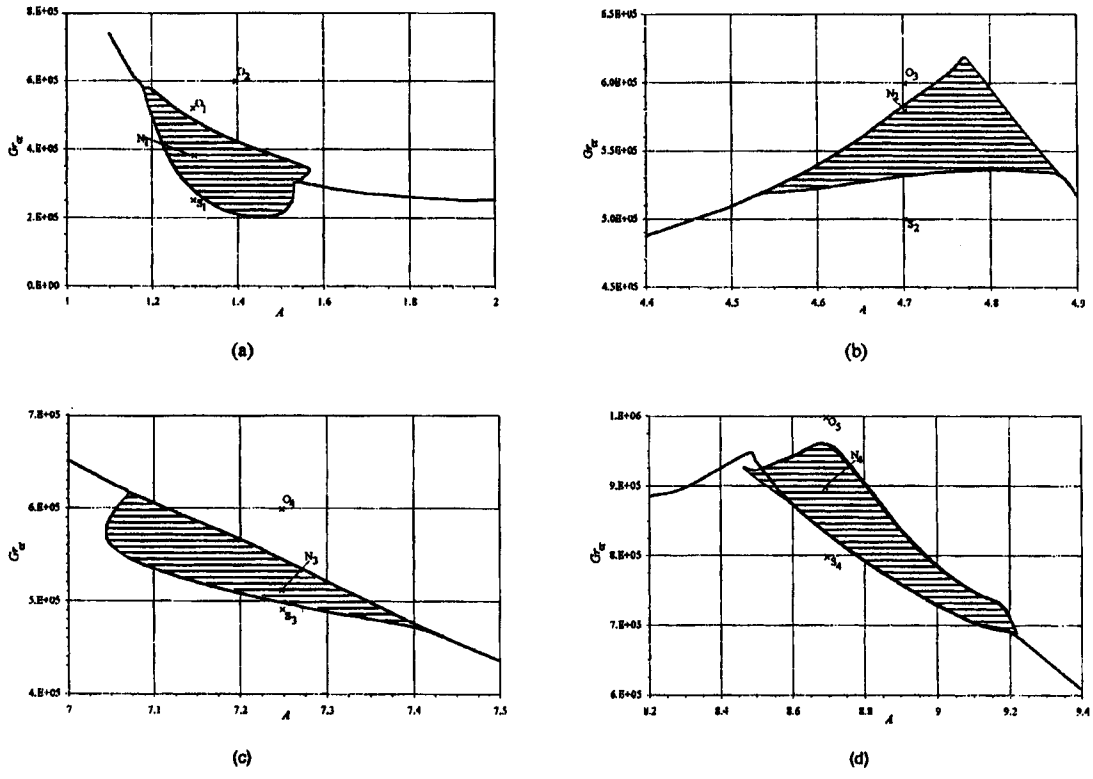

FIGURE 1 Fragments of the stability diagram containing regions of the stability of steady state flows with broken central symmetry. The non-symmetric steady state flows are stable inside the shadowed regions. (a) single-roll steady state flows, (b) two-roll steady state flows, (c) three-roll steady state flows, (d) four-roll steady state flows.

such that the lower neutral stability curve of the steady non-symmetric states is located slightly below the neutral curve. This curve corresponds to the transition from symmetric to non-symmetric four-roll steady states (Fig. 1(d)).

Examples of the transition from centrally symmetric to non-symmetric steady state flows are shown in Figures 2–5 for single-, two-, three- and four-roll states, respectively. Figures 2 and 3 also illustrate comparison between calculations carried out by the Galerkin and the finite volume methods. In case of the Galerkin method a single non-symmetric steady state flow (corresponding to a certain branch of multiple steady states) was calculated by the time-marching integration of the dynamical system (14) at a value of the Grashof number above the corresponding neutral curve. A subcritical centrally symmetric flow with an added small non-symmetric perturbation was used as an initial guess for this calculation. After one non-symmetric steady state flow was calculated, all other non-symmetric solutions were obtained by the parameter continuation technique. In the case of the finite volume method centrally symmetric flow was calculated using the result of the Galerkin method as an initial guess. Then the increase of the Grashof number above the corresponding critical curve and further time-marching calculations leads to the break of symmetry and the convergence to non-symmetric steady state flow.

Comparisons of the results obtained by the two independent numerical approaches (Figs. 2 and 3)

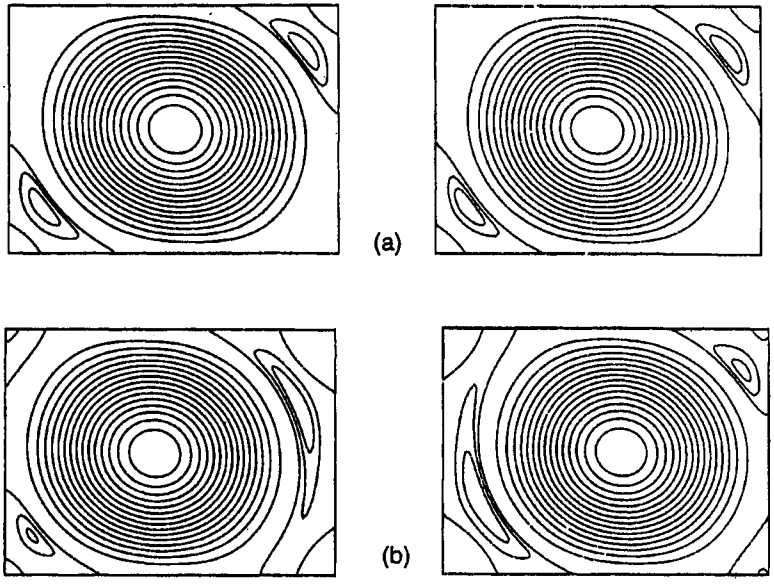

FIGURE 2 Single-roll steady state flows. $A = 1.3$, $Pr = 0$. Calculation using the Galerkin (left frames, 30×30 basis functions) and the finite volume (right frames, 75×75 uniform grid) methods. (a) $Gr = 2.5 \times 10^5$ (point S_1 in Fig. 1a), (b) $Gr = 3.8 \times 10^5$ (point N_1 in Fig. 1a).

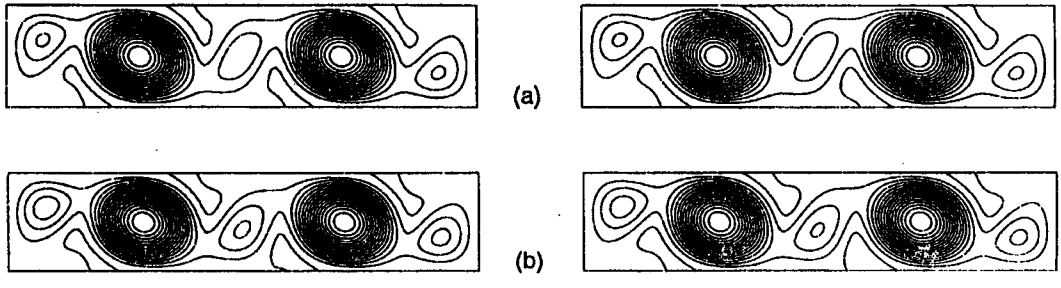

FIGURE 3 Two-roll steady state flows. $A = 4.7$, $Pr = 0$. Calculation using the Galerkin (left frames, 50×20 basis functions) and the finite volume (right frames, 200×50 uniform grid) methods. (a) $Gr = 5 \times 10^5$ (point S_2 in Fig. 1b), (b) $Gr = 5.8 \times 10^5$ (point N_2 in Fig. 1b).

illustrate two possibilities of the pitchfork bifurcation. In the case shown in Figure 2(b) the nonsymmetric flows calculated by the Galerkin and the finite volume methods bifurcate to different branches of the pitchfork. One of the results can be transformed into another after rotation by 180° about the cavity center. In the case shown in Figure 3(b) both calculations arrive at the same branch of the pitchfork.

Note that calculation of bifurcations of central-symmetry-breaking by two independent numerical approaches approves the existence of such steady bifurcations. An analogous comparison can also be performed for the upper parts of the described regions of stability corresponding to the onset of the oscillatory instability. In the case of the supercritical Hopf bifurcation the weakly nonlinear approximation of oscillatory flows (16) can

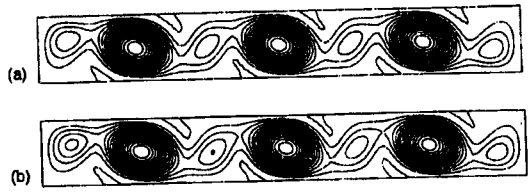

FIGURE 4 Three-roll steady state flows. $A = 7.25$, $\mathrm{Pr} = 0$. Calculation using the Galerkin method, 60×20 basis functions. (a) $\mathrm{Gr} = 4.9 \times 10^5$ (point S_3 in Fig. 1c), (b) $\mathrm{Gr} = 5.2 \times 10^5$ (point N_4 in Fig. 1c).

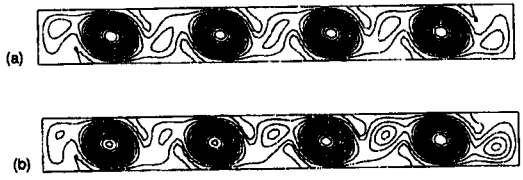

FIGURE 5 Four-roll steady state flows. $A = 8.7$, $\mathrm{Pr} = 0$. Calculation using the Galerkin method, 60×20 basis functions. (a) $\mathrm{Gr} = 8 \times 10^5$ (point S_4 in Fig. 1d), (b) $\mathrm{Gr} = 9 \times 10^5$ (point N_4 in Fig. 1d).

be compared with the result of solution of the full unsteady problem. The corresponding examples are shown in Figures 6 and 7. It is seen that the patterns of the oscillatory flow approximated asymptotically (the result of the Galerkin method) are similar to the corresponding patterns calculated by the finite volume method (the solution of the full unsteady problem). Besides the patterns of the oscillatory flows, the frequencies of oscillations can also be compared. The results are summarized in Table I which shows the critical values Gr_{cr} and ω_{cr}, the parameters μ and τ of the asymptotic approximation (16), and values of the frequencies approximated asymptotically (the Galerkin method) and calculated *via* the time-marching calculations (the finite volume method) for points $O_1 - O_5$ in Figure 1. It is seen that in the cases of supercritical bifurcations ($\mu > 0$) the results of the asymptotic approximations are close to the calculated values of the circular frequency. This provides another validation of the weakly nonlinear analysis.

The weakly nonlinear approximation (16) cannot be applied in the cases of subcritical bifurcation and for large supercriticalities. In these cases the solution of the full unsteady problem is the only way to calculate the oscillatory flows. The corresponding examples are shown in Figures 8 and 9. Figure 8 shows oscillations corresponding to the point O_4 (Fig. 1(c)) which result from the subcritical Hopf bifurcation. The absolute value of the parameter μ in this case is rather small (see Tab. I) which indicates on that the subcriticality depth is relatively small. Because of this, a

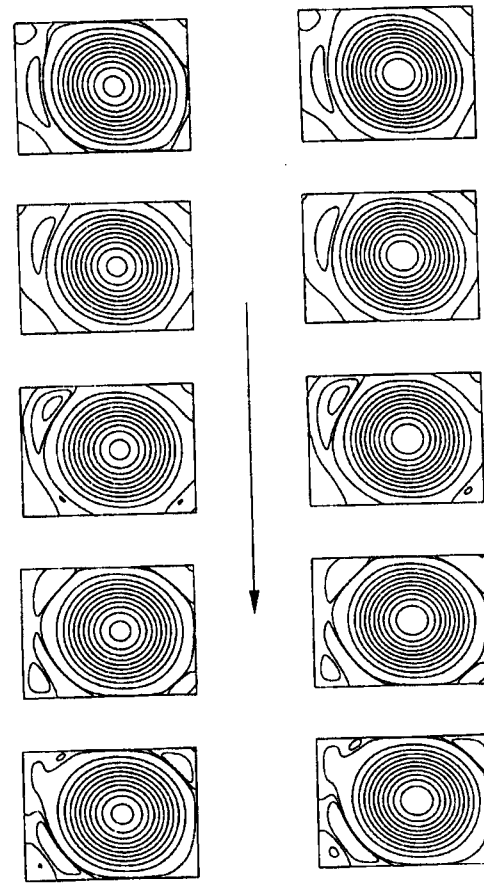

FIGURE 6 Snapshots of the streamlines (plotted over the time intervals equal to $T/5$) corresponding to the slightly supercritical flow at $A = 1.3$, $\mathrm{Pr} = 0$, $\mathrm{Gr} = 5.2 \times 10^5$ (point O_1 in Fig. 1a). Left frames – calculation using the Galerkin method, 30×30 basis functions; right frames – calculation using the finite volume method, 75×75 uniform grid.

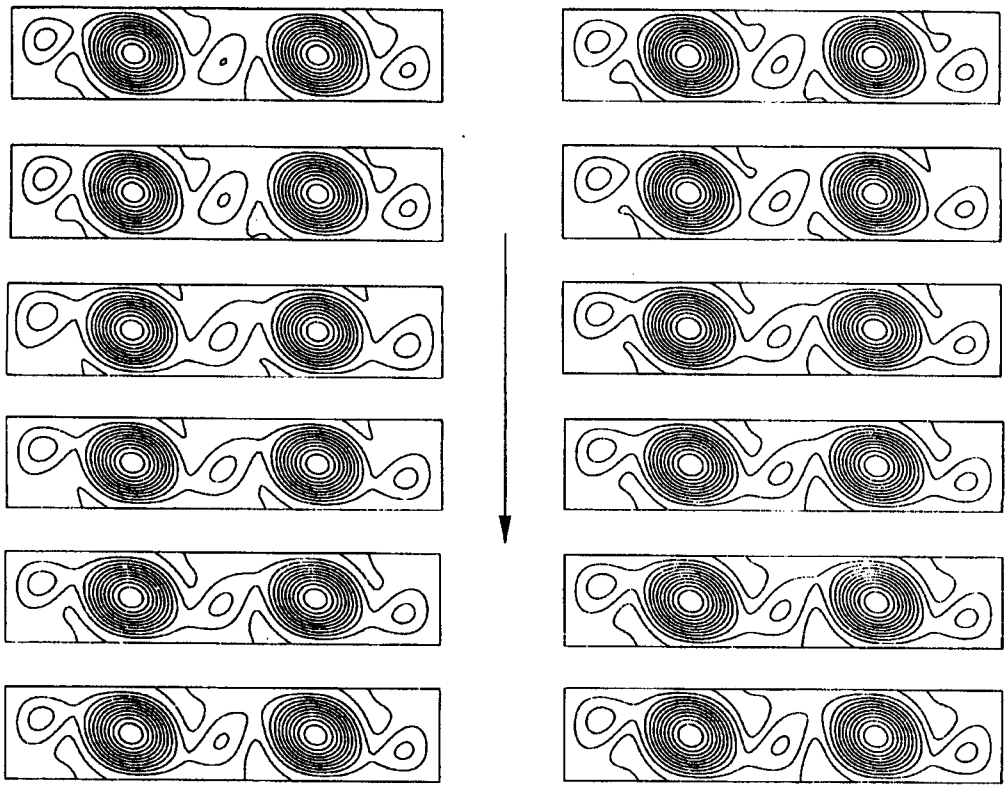

FIGURE 7 Snapshots of the streamlines (plotted over the time intervals equal to $T/6$) corresponding to the slightly supercritical flow at $A = 4.7$, $Pr = 0$, $Gr = 6 \times 10^5$ (point O_3 in Fig. 1b). Left frames – calculation using the Galerkin method, 60×20 basis functions; right frames – calculation using the finite volume method, 200×50 uniform grid.

TABLE 1 Results of the linear and weakly nonlinear analysis of the Hopf bifurcations (Galerkin method) and the frequencies of oscillations calculated *via* the solution of the full unsteady problem (finite volume method)

A	$Gr_{cr} \times 10^{-5}$	ω_{cr}	μ	τ	$Gr \times 10^{-5}$	ω (asymptotic approximation, Galerkin method)	ω (full unsteady problem, finite volume method)
1.3	4.831	2392	700.2	−0.001410	5.2	2583.	2576.
4.7	5.830	799.4	10329.	−0.01744	6.0	823.	816.
7.25	5.437	137.3	−0.3271	0.000520	6.0	–	270.
8.7	9.597	733.0	27906.	−0.024419	10.0	760.	754.

significantly large amplitude of oscillations can be found at points which are considerably above the corresponding neutral curve (like point O_4 in Fig. 1(c)). Oscillations shown in Figure (9) correspond to point O_2 in Figure 1(a). In this case the oscillations remain single-periodic, but the oscillatory flow at such supercritically already cannot be approximated by the first term of the expansion (16).

Knowledge on the existence of the central-symmetry-breaking steady bifurcations permits to interpret the experimental results of [10] obtained for the convection of mercury ($Pr = 0.026$) in the cavity with the aspect ratio and the width ratio

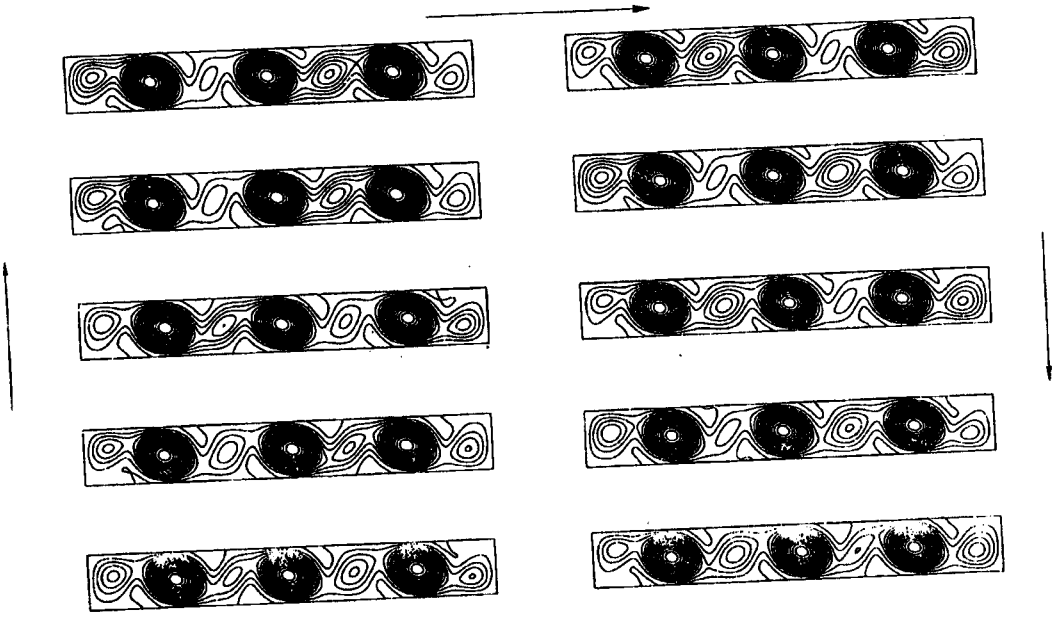

FIGURE 8 Snapshots of the streamlines (plotted over the time intervals equal to $T/10$) corresponding to oscillatory flow at $A = 7.25$, $\mathrm{Pr} = 0$, $\mathrm{Gr} = 6 \times 10^5$ (point O_4 in Fig. 1c) in case of subcritical bifurcation. Calculation using the finite volume method, 300×50 uniform grid.

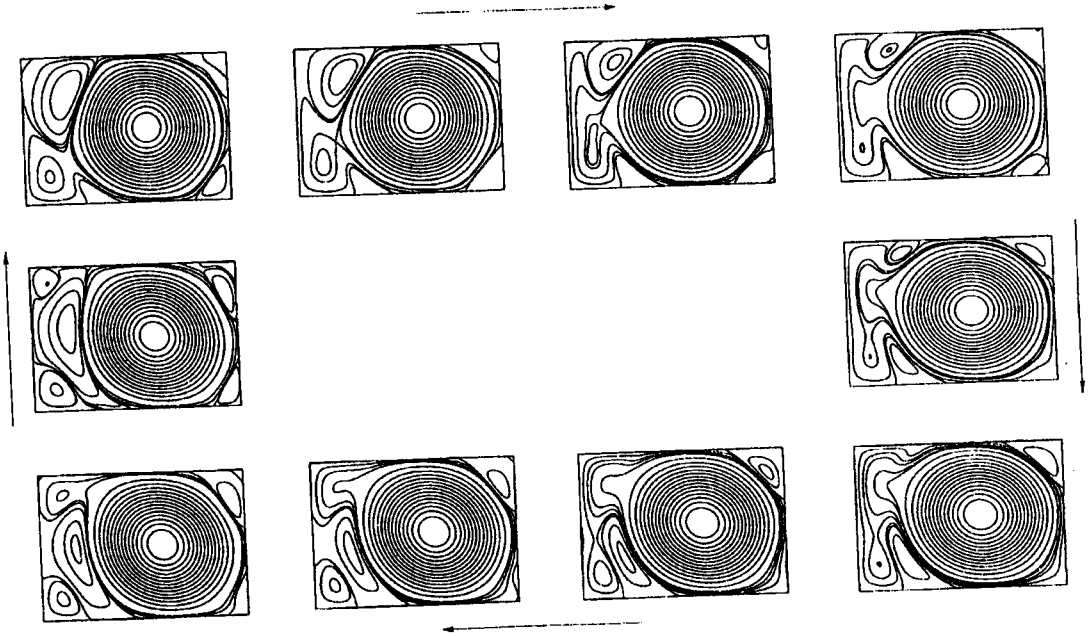

FIGURE 9 Snapshots of the streamlines (plotted over the time intervals equal to $T/10$) corresponding to oscillatory flow at $A = 1.4$, $\mathrm{Pr} = 0$, $\mathrm{Gr} = 6 \times 10^5$ (point O_2 in Fig. 1c) at large subcriticality. Calculation using the finite volume method, 100×100 uniform grid.

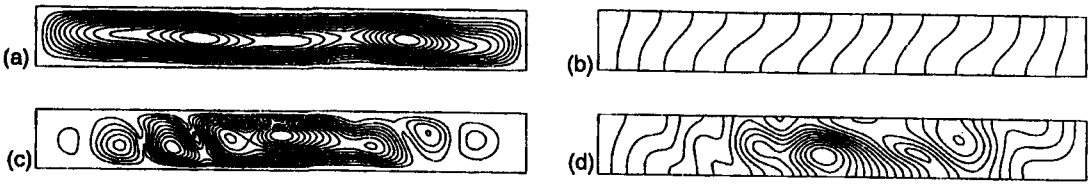

FIGURE 10 Streamlines (a), isotherms (b), amplitude of the most unstable perturbations of the stream function (c) and the amplitude of the temperature perturbation (d) for non-symmetric two-roll steady state. $A = 8$, $\mathrm{Pr} = 0.026$, $\mathrm{Gr} = 1.45 \times 10^5$. Calculation using the Galerkin method, 60×20 basis functions.

(width/height) W equal to 8. The experimental results (recalculated for the present definition of Gr and ω) for the onset of the oscillatory instability yield $\mathrm{Gr}_{cr}^{\mathrm{exp}} = 1.77 \times 10^5$ and $\omega^{\mathrm{exp}} \approx 32.6$. The non-dimensional value of ω^{exp} was estimated from the first peak of the frequency power spectrum shown in Figure 9b of [10] with the use of the time scale H^2/ν, where $H = 0.81$ cm (reported in [10]) and the value of the kinematic viscosity ν of mercury at 23°C was taken as $\nu = 1.2 \times 10^{-6}\,\mathrm{m}^2/\mathrm{c}$. We assume here that the second peak of the frequency power spectrum in Figure 9(b) of [10] is a harmonic of that one corresponding to the smallest frequency.

According to the results of [4–6], several stable steady states are possible at $A = 8$. Since only temperature oscillations were measured in the experiments [10], it is unknown which one of the multi-roll steady states was observed. Therefore, to compare with the experimental results, it is necessary to calculate the critical parameters for each possible branch of the steady state flows. The dependence $\mathrm{Gr}_{cr}(\mathrm{Pr})$ reported in [6] showed that comparison with the experiment should be done for exactly the same value of the Prandtl number. Therefore, the fixed value of the Prandtl number of mercury $\mathrm{Pr} = 0.026$, reported in [10], was used in the present computations. Calculations starting from the zero Grashof number, at the fixed value of the aspect ratio $A = 8$, lead to the stable centrally symmetric three-roll steady state flow. This flow becomes oscillatory unstable at $\mathrm{Gr}_{cr}^{(3)} = 2.05 \times 10^6$ with the critical circular frequency $\omega_{cr}^{(3)} = 228.2$. A centrally symmetric four-roll steady state flow at $A = 8$ can be calculated by the following computational path. First, the Grashof number is increased up to 10^6 at $A = 9$, and then the aspect ratio is decreased to $A = 8$. The critical parameters of the four-roll steady state flow are $\mathrm{Gr}_{cr}^{(4)} = 1.16 \times 10^6$ and $\omega_{cr}^{(4)} = 165.5$. Neither of these critical points fit the experimental result of [10].

Study of the stability of the centrally symmetric two-roll steady state flows shows that they become unstable with respect to a steady bifurcation ($\omega_{cr}^{(2)} = 0$) for $A \gtrsim 7.7$. Time marching integration of the dynamical system (14) for $A > 7.7$ with the use of the two-roll steady state at $A = 7.7$ as an initial guess yields a two-roll steady state flow with a broken central symmetry. The region of stability of non-symmetric two-roll steady state flows extends beyond the value $A = 8$. The critical parameters at $A = 8$, corresponding to the onset of the oscillatory instability of this steady state branch, are $\mathrm{Gr}_{cr}^{(2)} = 1.45 \times 10^5$ and $\omega_{cr}^{(2)} = 34.96$. These parameters are much closer to the experimental results of [10]. The patterns of the steady flow and the corresponding most unstable perturbation are plotted in Figure 10.

The weakly nonlinear analysis of the above bifurcation permits an additional comparison with the experimental observations. The parameters of the asymptotic expansion (16) were found to be $\mu = 5477$ and $\tau = 0.004836$. A positive value of the parameter τ means that the frequency of the oscillations decreases (the period increases, see (16c)) with the increase of the Grashof number. Calculation for $\mathrm{Gr} = 1.77 \times 10^5$ yields $\omega = 33.98$,

which is closer to the experimental result than $\omega_{cr}^{(2)} = 34.96$. Thermal probes in the experiment [10] were inserted along the central plane $y = 0.5$, $x = A/2$ of the cavity. The non-dimensional amplitude of the temperature oscillations at the center of the cavity ($y = 0.5$, $x = A/2$), was estimated using (16c), and found to be approximately 1% of its averaged value. This yields a possible explanation for the difference between the experimental and the calculated critical Grashof numbers. Since only finite amplitude of the temperature can be indicated in an experiment, it is possible that oscillations with smaller amplitudes were not registered by the introduced thermal probes used.

The results described support the assumption made in [6] which stated that for convection of low-Prandtl number fluids, the two-dimensional stability analysis provides results comparable with the experimental data if the width ratio (width/height) of the experimental container is sufficiently large.

5. CONCLUSIONS

Use of two independent numerical approaches (based on the spectral Galerkin and the finite volume methods) allowed us to obtain validated results on steady bifurcations of the central symmetry breaking and on the oscillatory instability of non-symmetric steady state flows. It should be emphasized that both numerical techniques used here complement each other. The complete analysis of stability and calculations of the stability diagrams can be carried out only by the spectral Galerkin method. The finite volume method provides not only validation of the obtained stability results but also permits calculations in cases of subcritical bifurcations and at large supercriticalities. Besides this, results of the Galerkin method can be used as an effective initial guess for the time-marching computations of the finite volume method.

Examples of the steady and oscillatory non-symmetric flow patterns shown in Figures 2–8, as well as the parameters shown in Table I, can be proposed as benchmark cases for numerical methods used for analysis of the stability of fluid flows. Correct calculation of steady and unsteady bifurcations requires sufficiently good resolution of both flow and its most unstable perturbation. Conservation properties of a numerical method also seem to be a necessary requirement for correct numerical modeling of instabilities of fluid flows.

The explanation of the experimental result of [10] proposed here, is in contradiction with the interpretation given in [10] which stated that the observed oscillatory instability has completely three-dimensional origin. The present results show that the two-dimensional model of the phenomenon yields results which are close to the experimental ones. The assumption is that (in this particular experiment) fluid motion in the width direction, which obviously exists in the real three-dimensional flow, has no significant influence on the transition from steady to oscillatory regime. This supports the assumption made in [6] which stated that two-dimensional models of the low-Prandtl-number fluids convection can reproduce the experimental results in cases when the width ratio of the experimental container is sufficiently large.

Acknowledgements

This research was supported by the German-Israeli Foundation for Scientific Research and Development, grant No. I-284.046, 10/93.

References

[1] Roux, B. (Ed.). (1990). Numerical simulation of oscillatory convection in low-Pr fluids: A GAMM workshop. *Notes on Numerical Fluid Mechanics*, Vieweg, Braunschweig, Vol. 27.

[2] Braunsfurth, M. G. and Mullin, T. (1996). An experimental study of oscillatory convection in liquid gallium. *Journal of Fluid Mechanics*, **327**, 199–219.

[3] Gelfgat, A. Yu., Bar-Yoseph, P. Z. and Yarin, A. L. (1997). On oscillatory instability of convective flows at low Prandtl number. *ASME J. Fluids Engineering*, **119**, 823–830.

[4] Gelfgat, A. Yu., Bar-Yoseph, P. Z. and Yarin, A. L. (1998). Patterns of bifurcating convective flows in long

horizontal cavities. *Advances in Computational Heat Transfer*, (de Vahl Davis, G. and Arínc, F. Eds.) Begell House 1998, (to appear).

[5] Gelfgat, A. Yu., Bar-Yoseph, P. Z. and Yarin, A. L. (1998). Multiplicity and stability of steady convective flows in laterally heated cavities. *Proc. 11th Int. Heat Transfer Conference, to be held in Kyongju, Korea*, August 23–28, 1998.

[6] Gelfgat, A. Yu., Bar-Yoseph, P. Z. and Yarin, A. L. (1998). Stability of multiple steady states of convection in laterally heated cavities. (submitted for publication).

[7] Gelfgat, A. Yu. and Tanasawa, I. (1994). Numerical analysis of oscillatory instability of buoyancy convection with the Galerkin spectral method. *Numerical Heat Transfer, Part A*, **25**, 627–648.

[8] Gelfgat, A. Yu., Bar-Yoseph, P. Z. and Solan, A. (1996). Stability of confined swirling flow with and without vortex breakdown. *Journal of Fluid Mechanics*, **311**, 1–36.

[9] Patankar, S. V. and Spalding, D. B. (1972). A calculation procedure for heat, mass and momentum transfer in three-dimensional parabolic flows. *Int. J. Heat Mass Transfer*, **15**, 1787–1806.

[10] Pratte, J. M. and Hart, E. (1990). Endwall driven, low Prandtl number convection in a shallow rectangular cavity. *J. Cryst. Growth*, **102**, 54–68.

[11] Hopf, E. (1942). Abzweigung Einer Periodischen Losung von Einer Stationaren Losung eines Differentialsystems. *Ber. Verh. Sachs. Acad. Wiss. Leipzing Math-Nat.*, **94**, 3–22.

[12] Hassard, B. D., Kazarinoff, N. D. and Wan, Y.-H. (1981). *Theory and Applications of Hopf Bifurcation*. London, Math. Soc. Lecture Note Series, Vol. 41.

[13] Janssen, R. J. A., Henkes, R. A. W. M. and Hoogendoorn, C. J. (1993). Transition to time-periodicity of a natural convection flow in a 3D differentially heated cavity. *Int. J. Heat Mass Transfer*, **36**, 2927–2940.